Audio Engineering Society

Conference Paper

Presented at the 2022 International Conference on
Audio for Virtual and Augmented Reality
2022 August 15–17, Redmond, WA, USA

Digital Twin of a Head and Torso Simulator: Validation of Far-Field Head-Related Transfer Functions with Measurements

Setare Hajarolasvadi[1], Brittany Essink[2], Pablo F. Hoffmann[1], Alan Ng[2], Ulrik Skov[2], and Sebastian Prepeliță[1]

[1]*Reality Labs Research, 8747 Willows Road, Redmond, Washington, 98052, USA*
[2]*Reality Labs, 1 Hacker Way, Menlo Park, SUN103, California, 94025, USA*

Correspondence should be addressed to Setare Hajarolasvadi (setarehajarola@fb.com)

ABSTRACT

Developing high-fidelity digital twins of head and torso simulators (HATS) provides us with reliable simulations that could replace tedious measurements and facilitate the rapid and efficient design of AR/VR products. In this paper, we aim to develop and validate a digital twin of the Brüel and Kjær high-frequency HATS Type 5128. The digital twin uses an accurate scan of the HATS and captures the behavior of the ear simulator (Type 4620), including the full average human ear canal geometry and a termination coupler emulating an average eardrum impedance response. As a natural first step, finite-element acoustic simulations in COMSOL are set up to validate the far-field head-related transfer function (HRTF) with measurements for three spatial directions in the horizontal plane. To increase the confidence in the validation results, a rough convergence study is conducted for the simulations, and measurements are compared against the manufacturer's reference measurements. Finally, we show how validation studies may be improved by investigating some of the commonly-used modeling assumptions.

1 Introduction

Head-related transfer functions (HRTFs) contain information that describes how the head and torso of an individual interact with incident sound fields. Therefore, HRTFs are an essential component in the design of audio devices. Recall that the HRTF is a complex frequency ratio between the response at the ears and the free-field response, which corresponds to response at the center of the head with the head absent [1]. In other words, for an omnidirectional point source located at (r,ϕ,θ) relative to the head center, an HRTF at a frequency f is defined as

$$H(r,\phi,\theta,f) = \frac{P(r,\phi,\theta,f)}{P_0(r,f)} \tag{1}$$

where, P represents the Fourier transform of the sound pressure at a location of interest in the external ear, and P_0 represents the sound pressure at the head center with the head absent. r,ϕ,θ indicate the distance, azimuth and elevation [2].

Unless the device design is tailored to an individual, head and torso simulators (HATS) can be used to provide a generic HRTF [3]. Thus, developing a digital

twin of a HATS serves to frontload render stack architectural, design and optimization decisions through simulations. Moreover, it ensures the reliability of data informing various stages of design, optimization and troubleshooting. This manuscript reports on the development and validation of a digital twin for the Brüel and Kjær (B&K) high-frequency HATS Type 5128.

When properly validated, numerical simulations may serve as an efficient replacement for tedious measurements [4, 5]. The majority of validation studies in this area have focused on HRTFs at the blocked meatus [6]. However, the acoustics of the ear canal and its coupling to external sound sources are of interest for more natural auditory perception in virtual environments [1, 7]. Fewer works exist where the ear canal geometry has been explicitly modeled in numerical simulations of the HRTFs [8, 9, 7, 10, 11]. The existing works, however, deal with human subjects; they mostly focus on the effects of morphological parameters on HRTFs or aim to create a database of ear canal geometries. This work primarily focuses on controlled validation studies of a head and torso simulator and attempts to identify, quantify and control possible sources of error in the process.

First, we briefly explain how an accurate geometry for the HATS and the ear canal is obtained. We also discuss how the performance of the ear simulator is captured in the digital twin through introducing equivalent impedances. In the next part, we focus on the validation studies, which consist of the HRTF measurements and numerical simulations in COMSOL Multiphysics® [12]. In the last section, we will show how reconsidering some of the common modeling assumptions improves validation studies.

2 Methods

In this section, we present the essential preliminary steps taken to ensure that a high-fidelity digital twin is developed. First, we discuss validation of the Computer-Aided Design (CAD) drawing provided by B&K against an in-house scan. Then, capturing the acoustic response of the ear simulator is discussed in two steps: (1) embedding ear canal's geometry in the original CAD drawing, and (2) using reduced-order impedance models to replicate the transfer impedance.

2.1 HATS CAD Drawing Validation

A CAD drawing provided by B&K was used to include the topology of the HATS in the model. It should be noted that this CAD drawing did not include the geometry of the ear canal. To minimize sources of error, the CAD drawing was validated against an in-house scan of the HATS that the HRTF measurements were conducted on. This scan was obtained by using an accurate blue-light scanner (Space Spider, Artec 3D). The resulting mesh, consisting of 76 million triangles, was then cleaned of artifacts and decimated (to 1 million triangles) to facilitate the next steps. The scanning pipeline was previously validated to yield highly accurate results especially for the ears (error less than 1 mm) and head - see, e.g., Ref.[4].

A triangulated mesh of the original CAD drawing was aligned to the decimated scanned mesh using the iterative closest point (ICP) algorithm. The two-sided Hausdorff distance was then calculated using Meshlab (v.2021.10) [13]. The Hausdorff distance will account for errors due to scanning, mesh alignment, and operator's expertise. The results indicate that error was within 5 mm for the surfaces of interest (Fig. 1). Similar results were obtained when the process was repeated for two other less-decimated versions of the scanned mesh (2 and 5 million triangles). It should be noted that some surfaces (e.g. the side handle, mouth protrusion, etc.) exist in one mesh but not the other. Error levels will naturally overshoot in these regions. However, these features do not affect HRTFs and are not of interest for the purposes of this validation study. Finally, note that the geometrical error is below 1 mm at the regions of most importance for HRTFs (ears, head and shoulders).

2.2 Reconstruction of Ear Canal Geometry

A notable feature of the Type 4.3 ear simulator is that it includes the full average ear canal geometry (defined and specified in the standard [14]). In order to capture the full geometry in the model for HRTFs captured at the eardrum, it is imperative to embed an accurate representation of this average ear canal in the existing CAD drawing.

The geometry of the ear canal was reconstructed per the guidelines of ITU-T Rec.P.57 [14]. The document specifies an average ear canal geometry using several cross-sectional areas normal to the ear canal's curved

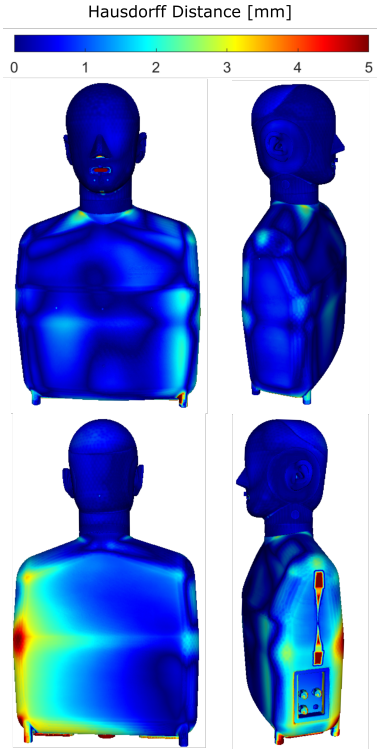

Fig. 1: HATS CAD drawing validation against the least decimated mesh (5 million triangles) resulting from 3D scanning. The contour shows a one-sided Hausdorff distance, with the maximum set to 5 millimeters.

centerline. Each cross section is defined with a set of points in a plane. The coordinates of these points were imported in the existing CAD drawing and Studio Spline (Siemens NX) was then used to reconstruct the curves (Fig. 2a). Next, a local coordinate system was defined for each cross section using a set of orthonormal vectors, as outlined in [14]. The local coordinate systems were then used to align the cross sections and reconstruct the 3D geometry (Fig. 2b). Two of the pinna's closest cross sections to the concha bottom were used to ensure a smooth connection between the pinna and the ear canal.

2.3 Capturing the Coupler's Transfer Impedance

The ear canals of the B&K mannequin can be fitted with a termination coupler designed to reproduce the transfer function of the inner ear of an average human adult [14]. To include the acoustical effects of the

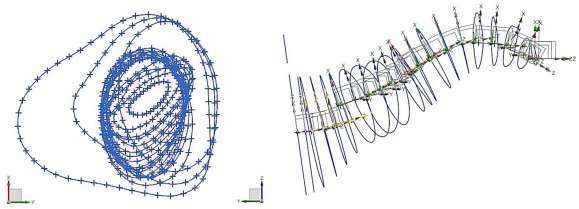

(a) Cross sections. **(b)** Local coordinates and alignment.

Fig. 2: Reconstruction of the ear canal geometry.

coupler in the final FEM model, a calibration exercise was conducted.

The portion of the coupler containing the main complex geometrical features was CT scanned. A corresponding CAD drawing was then prepared and used to develop a continuous parameter model in COMSOL by coupling the *Thermoviscous Acoustics* interface (applied to cavities) with the *Pressure Acoustics* interface (applied to the rest of the domain). An equivalent impedance is specified at the location of the measurement microphone. The coupler is characterized in terms of its acoustical transfer impedance for a constant-volume displacement source using a *Frequency Domain* study. A reference volume must be used for the calibration of the ear simulator [14]. The shape and dimensions of this calibration volume were chosen such that the numerical transfer impedance would fit that measured by B&K. Acoustically, the coupler's transfer function could be captured by imposing equivalent termination impedances on appropriate surface areas at the end of ear canal. These impedance boundary conditions will replicate the measurement microphone as well as the losses within the coupler. As such, a lumped parameter model was developed for the coupler. In this model, the CT scanned portion of the geometry was removed. Instead, termination impedances representing the measurement microphone and losses were selected on appropriate surface areas such that the transfer impedance of this new model would match that of the continuous parameter model.

Finally, these termination impedances were integrated in the HATS model by applying impedance boundary conditions to surfaces of similar cross-sectional area at the end of the ear canal.

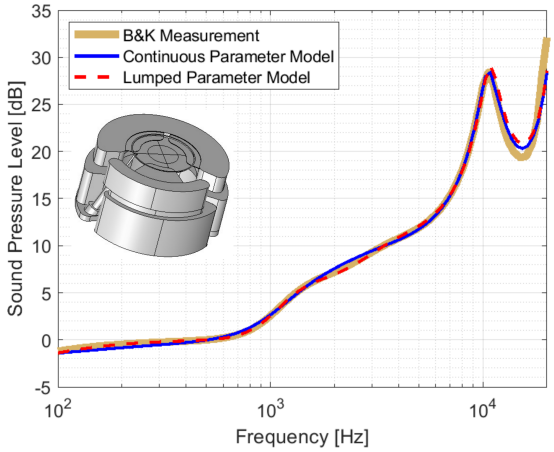

Fig. 3: Calibration of the acoustics of the coupler: transfer impedance for ear simulator Type 4620 relative to the reference frequency 500 [Hz]. The insert shows the CAD drawing of the CT scanned portion.

3 Validation

In this section, we discuss the HRTF measurements and simulations.

3.1 Measurements

Measurements were conducted in an anechoic chamber using a logarithmic sweep (50 Hz to 20 kHz) with a sampling rate of 48 kHz and a duration of 1 s. The speaker used is a modified version of a Meyer MM-4XP. To ensure proper alignment of the sources and receivers, the laser-based system for accurate positioning of the free-field microphone and HATS was calibrated before measurements. The estimated alignment error was below 1°. Fig. 4a shows the measurement setup. Free-field measurements were done with a free-field microphone (GRAS 46BF 1/4" LEMO) positioned at the center of the loudspeaker-array arc. Both platform and microphone stand were covered in absorptive material to reduce unwanted reflections from the setup. The HATS was also aligned with the sagittal, horizontal and frontal laser beams. Measurements at the Drum Reference Point (DRP) were conducted in the horizontal plane for 0°, 45° and 90° azimuth angles at 0° elevation. After deconvolving the free-field measurements from that of the HATS, the frequency response was computed in $1/12^{th}$ octave bands. Figure 4b shows the HATS HRTF at 0° azimuth against the range of B&K's

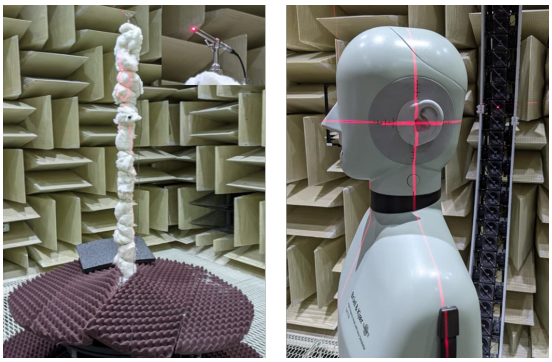

(a) Measurement setup. Left: free-field measurement. Right: DRP measurement.

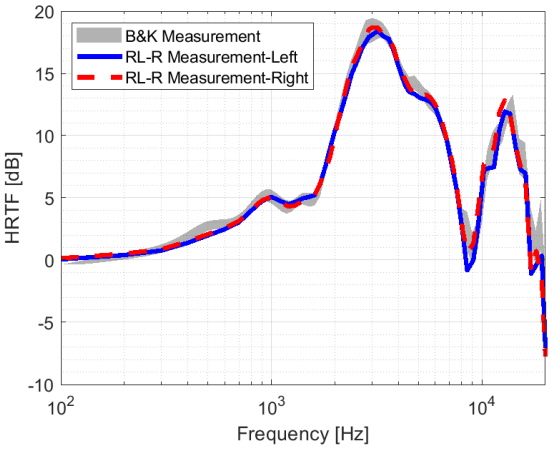

(b) HATS measured HRTF.

Fig. 4: HRTF measurements for HATS: (a) free-field measurements and HATS measurements, and (b) in-house HRTF measurements compared to $\pm 2\sigma$ of B&K data for 23 HATS in the frontal direction.

certified responses from all 23 B&K 5128 HATS that Meta currently owns (data includes both left and right ears). The grey shaded area shows the two sigma region, where sigma is the sample standard deviation. No repeated measurements were acquired to quantify measurement error. Nevertheless, the cross validation with the B&K measurements from Fig. 4b can be seen as a reproducibility study indicating a small amount of bias and random error for the frontal direction.

3.2 Simulations

Simulations were set up to reflect the test rig as closely as possible. The Cartesian coordinate system is that

most commonly used for HRTFs with the origin located at the head center. The final CAD drawing, including the ear canal geometry and the termination impedances representing the coupler, is used in the simulations (Fig. 5). The COMSOL model uses a frequency-domain Finite Element Method (FEM) solver and the *Pressure Acoustics, Frequency Domain* interface. The model discretizes the Helmholtz equation in three dimensions. The HATS, treated as a perfectly rigid scatterer, is surrounded by a spherical air domain with a radius of 45 cm. The simulation domain is truncated using an absorbing boundary condition applied to the outer boundary of the sphere using COMSOL's *Spherical Wave Radiation* feature. A *Background Pressure Field* is applied to model a spherical wave of unit amplitude, propagating towards the manikin from a 2 m distance at the aforementioned spatial directions. Reduced-order models determined from the previous step are applied as *Serial Coupling RCL Impedance Boundary Condition* to integrate the coupler's behavior.

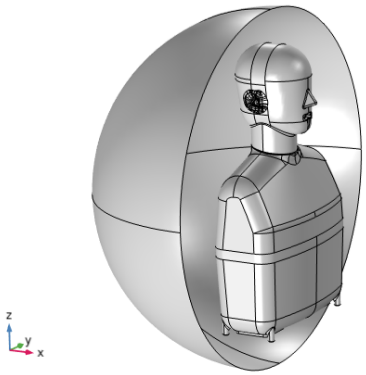

Fig. 5: Model setup in COMSOL. Absorbing boundary is partially hidden for better visualization.

It has long been established that the accuracy of the finite element solution for the Helmholtz problem depends on the wave number, k [15, 16]. For a specific wavelength λ and representative mesh size h, one can consider the parameter $n_{\text{res}} = \lambda/h$ as an indication of how well the wavelength has been resolved. In fact, the so-called rule of thumb, widely used in the literature, takes advantage of this parameter to adjust mesh size, h. The larger n_{res} is, the smaller the relative discretization error in the finite element solution should be. Note that this may not always be guaranteed due to pollution error - for more, the interested reader is referred to [17, 18]. When quadratic elements are used, as is the case in all simulations for the present work, the rule of thumb recommends for mesh size h to resolve at least 3 to 5 elements per wavelength [19, 20]. COMSOL's *Free Tetrahedral* feature is used to create an unstructured mesh with a maximum element size $h_{\max} = 6.86$ mm, corresponding to $n_{\text{res}} = 5$ for a frequency of 10 kHz. $h_{\max}$ is reduced for the ear canal domain to 5.72 mm (an equivalent of 6 elements per wavelength). A minimum element size of 0.05 mm is used for all domains.

The *Frequency Domain* study is set up along with a *Cluster Sweep* feature to parallelize computations. To avoid iterative error(s) and maintain robustness, a direct solver (MUMPS [21]) is used in all models. The simulations are memory-intensive. Simulation for each frequency bin uses 10 compute nodes (768 GB RAM) and takes approximately 45 minutes.

Average sound pressure magnitude is evaluated over left and right eardrum surfaces (< 60 mm^2 each). A normalization with the free-field pressure magnitude at the location of head center with the head absent gives the simulated HRTF. The magnitude of the free field response was calculated using the analytical form of the incident wave at a point from the source location.

3.3 Results

To compare the measured magnitude of the HRTF to that resulting from FEM simulations on the decibel scale, the following validation metric is used

$$\begin{aligned}\Delta(r,\phi,\theta,f) = 20\log_{10}(|H_m(r,\phi,\theta,f)|) \\ - 20\log_{10}(|H_s(r,\phi,\theta,f)|)\end{aligned} \tag{2}$$

where, $|H_m|$ and $|H_s|$ are HRTF magnitudes obtained through measurement and simulation, respectively.

Figure 6 shows the measured and simulated HRTF magnitudes as well as the validation metric Δ for the three spatial directions considered. For the frontal direction case, $\phi = 0^\circ$, we have also included the measurement data provided by B&K. Validation studies show that the simulation results capture the main features of measured HRTFs, with error levels bounded to 2 dB up to 7 kHz, except for the case of contralateral ear at 90° azimuth, which shows higher error levels beyond 3 kHz. Previous works [22, 23, 24, 25] have reported on higher measurement errors on the contralateral side

due to the effects of head shadowing, which causes significant decrease in the signal-to-noise ratio (SNR). Higher sensitivity to meshing has also been reported for HRTFs at the contralateral ear when using the boundary element method. For example, in [26], multiresolution meshing led to erroneous results in contralateral areas. Table 1 shows the maximum validation error $\Delta_{\max}$ from Eq. 2 for each spatial direction at the left and right eardrum. The frequency range is split in three intervals, $I_1 = [0.1, 3]$ kHz, $I_2 = [3, 12]$ kHz, $I_3 = [12, 20]$ kHz. Below 3 kHz, where the pinna has negligible effects on the HRTFs [27], $\Delta_{\max}$ remains relatively small. At frequencies above 12 kHz, both measurements [28, 29] and simulations [30] may be unreliable and $\Delta_{\max}$ increases significantly.

To gain confidence in the accuracy of the simulation results, a preliminary convergence study is conducted. Firstly, a code verification study is undertaken for the scattering from a rigid sphere where the estimated convergence rates for the employed FEM model matched the theoretical ones (results not shown). Then the convergence study for the simulated HRTFs is done as follows: the model is resolved on a sequence of progressively coarser meshes and it is shown that the error, relative to the finest mesh, decreases with each level of refinement. The maximal element size $h_{\max}$ was used to control the mesh size. For the finest mesh, $h_{\max} = 5.72$ mm in the ear canals and 6.86 mm in the remaining simulation domain, as mentioned previously. Five other meshes were systematically constructed such that $\frac{h^{i+1}_{\max}}{h^{i}_{\max}} = 1.1$; where $i \in \{0, 1, \ldots, 5\}$ represents the grid number with $i = 0$ corresponding to the finest grid. We track the convergence of sound pressure magnitude at both eardrums for all three spatial directions. A measure for the discretization error on each grid i may be defined as $\delta_i = 20 \log_{10} \frac{|P_i|}{|P_0|}$. For the sake of brevity, only results for the left ear at $\phi = 0°$ are presented.

Interval	$\phi = 0°$		$\phi = 45°$		$\phi = 90°$	
	L	R	L	R	L	R
I_1	1.20	0.73	1.21	1.51	1.30	1.71
I_2	4.37	3.20	3.84	3.17	2.66	4.34
I_3	6.98	7.73	5.51	7.01	6.16	9.17

Table 1: Maximum validation error of the HRTFs $\Delta_{\max}$ for each spatial direction at the left and right eardrum. See text for frequency intervals I_i.

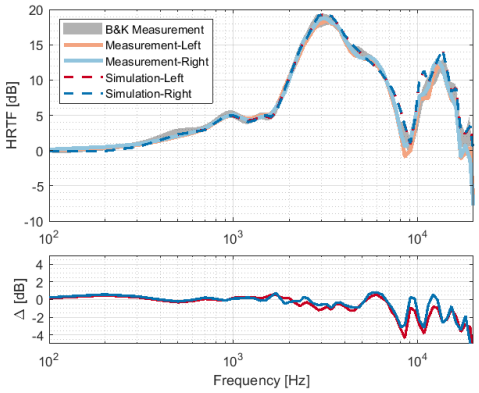

(a) $\phi = 0°, \theta = 0°$.

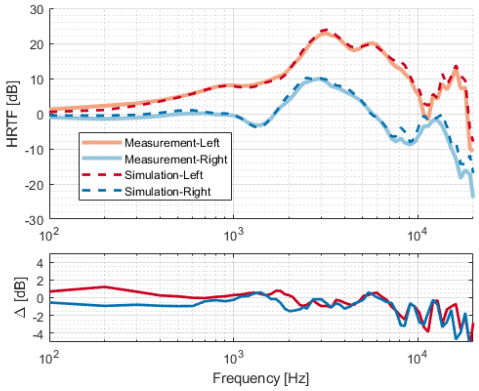

(b) $\phi = 45°, \theta = 0°$.

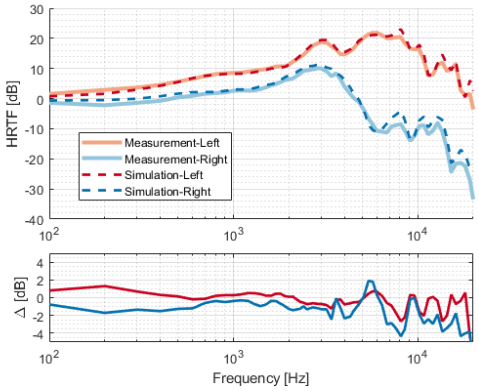

(c) $\phi = 90°, \theta = 0°$.

Fig. 6: Comparison of far-field HRTF magnitudes obtained by measurements and FEM simulations on the finest mesh, $h = 7.55$ mm for (a) 0°, (b) 45°, and (c) 90° azimuth. Δ is defined in Eq. 2.

Fig. 7 shows the discretization error, in this case, over the entire frequency range. It is observed that the error decreases, albeit in a non-monotonic fashion for some frequencies, as the mesh is refined. A similar overall trend was observed for all the other considered directions. Similar to other HRTF validation studies

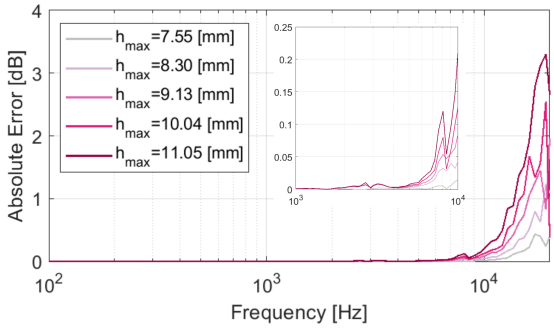

Fig. 7: Sample convergence plot for the left eardrum at 0° azimuth ($r = 2$ m) over the entire frequency range. The error is calculated between the magnitude of the simulation with the smallest grid ($h_{\max} = 5.72$ mm in the ear canals, $h_{\max} = 6.86$ mm for the remaining domain) and the simulated HRTFs for each grid. Insert zooms the 1-10 kHz frequency region of the main plot.

[6], results in Fig. 7 show that the discretization error should not be assumed negligible and should ideally be quantified. However, without providing error estimates, one could conclude from Fig. 7 that the existing rule of thumb of 5 elements per wavelength for the given quadratic elements (see section 3.2) seems to provide acceptable levels of discretization error up to 10 kHz: the change in the solution is below 0.05 dB when the grid is refined from $h_{\max} = 11.05$ mm.

4 Improving Validation Studies

In this section, we investigate two assumptions often used for far-field HRTF modeling and show the effect of each on the validation study previously presented.

4.1 Nature of the Acoustic Source

HRTFs are usually assumed independent of radius for radii larger than about 1 meter [31, 32] or slightly more (e.g., 1.5 meters [33]). In the asymptotic $r \to \infty$ limit, the incoming wavefront will be planar, perpendicular to the direction of arrival. Incident plane waves could be a

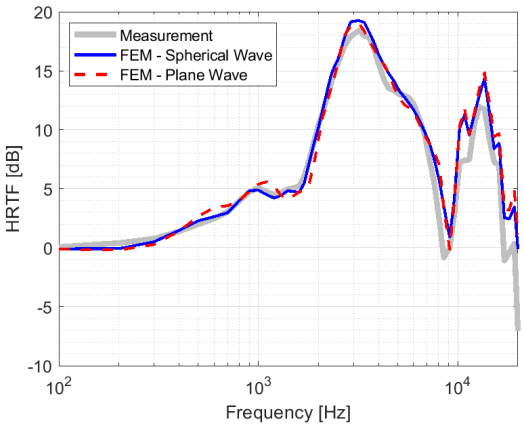

Fig. 8: Effect of the acoustic source's nature on the HRTF at 0° azimuth and elevation.

useful simplifying assumption for some far-field wave-based simulations. If HRTFs become independent of radius above, say, the employed $r = 2$ m radius, then the HRTF magnitude should be very close to the one simulated for $r \to \infty$.

Additional models, similar to the previous section, were developed with the exception that the acoustic source was assumed to be a plane-wave source. HRTF simulation results for HATS were then compared for the two cases. Fig. 8 shows the HATS HRTF for the two cases overlaid on the conducted measurements at 0° azimuth. The plots indicate that using a plane wave source leads to a low-frequency mismatch with measurements in the $[700, 1500]$ Hz frequency region while the rest of the transfer function remains almost unchanged. HRTFs for the other two spatial directions were minimally affected by the nature of the acoustic source. Note the numerical errors in this frequency range are negligible as supported by results in Fig. 7.

The observed difference in HRTF magnitude is likely due to the interaction of the incoming field with the torso since the torso affects HRTFs above approximately 700 Hz [27, 34]. This suggests that accounting for the nature of spherical wave fronts properly may be of more importance when the surfaces affecting the response are large enough and the surface normal is significantly aligned with the incident wave's direction of propagation. Results in Fig. 8 also show, assuming the wave-based model is a correct representation of reality, that the HRTF magnitude could change even after a 2 m radius for certain directions. It is unclear

whether such differences are audible or not; however, a study by Lenz [35] seems to indicate some perceptual significance.

4.2 Impedance of Ear Canal Walls

Here, we set up simulations similar to the previous section with the exception that the ear canal walls are no longer modeled as rigid. COMSOL's *Physiological Impedance (Human Skin)* feature is used to apply an impedance boundary condition to the ear canal walls. This impedance model is based on [36]. Note that the termination impedances of the coupler were kept at the termination of the ear canal. Fig. 9 shows a comparison of HRTFs at 0° azimuth at the left ear for the two different boundary conditions. It is observed that accounting for the ear canal wall impedance decreases the magnitude at the resonance peak, bringing simulation results closer to measurements and reducing the validation error.

Results in Fig. 9 suggest that the employed wave-based model does not account for some losses in the measurements. However, it is unclear if such losses occur in reality at the walls of the ear canal or at the termination of the ear canal. Similarly, the exact mechanism of generating such losses (e.g., boundary thermoviscous losses, viscous losses in the coupler, vibroacoustical losses in surrounding structures of the ear canal) is unclear.

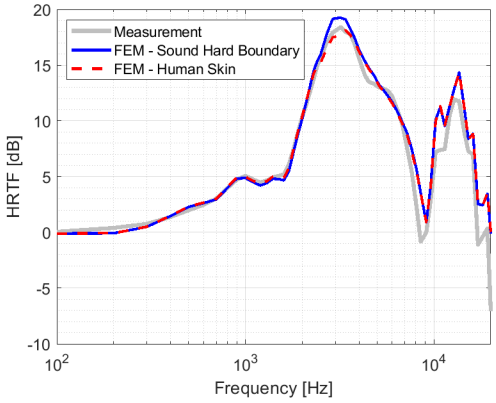

Fig. 9: Effect of ear canal wall impedance on the HRTF at 0° azimuth and 0° elevation.

5 Conclusion

In this paper, we developed a digital twin for the Brüel and Kjær high-frequency HATS Type 5128, fitted with a coupler which emulates a typical eardrum impedance. First, the HATS CAD drawing was validated against an in-house scan. Then, the physics of the coupler were embedded in the model in a two-step process: (1) reconstruction of the ear canal geometry and (2) replicating the coupler's transfer impedance through reduced-order models. HRTF measurements were conducted 2 meters away from the center of the head in an anechoic chamber at three spatial directions in the horizontal plane; FEM wave-based acoustic models in COMSOL were developed aiming to represent the test setup as closely as possible. To increase confidence in the simulation results, preliminary convergence studies were done by resolving the models on a sequence of progressively refined meshes. To increase the confidence in the measurements, the measurements were compared against the manufacturer's measurements for a collection of HATS mannequins in the frontal direction. Next, validation studies were conducted to assess the fidelity of the acoustic models. The main conclusions of the work are listed below:

- Simulations capture the main features of measured HRTFs, with error levels bounded to 2 dB up to 7 kHz, except for the case of contralateral ear at 90° azimuth, which shows higher error levels beyond 3 kHz.
- Relying on the simplified assumption of plane waves for far-field HRTF simulations may lead to low-frequency mismatch with measurements and higher error levels, as a result. The effect may be more significant when the surfaces affecting the response are large enough and the surface normal is significantly aligned with the incident wave's direction of propagation.
- Accounting for the ear canal wall impedance decreases resonance magnitude and introduces additional loss mechanisms. This brings the simulation results closer to measurements and reduces the validation error.

The present validation studies may be improved by properly quantifying and controlling several sources of error that typically exist in validation studies [6, 4] (e.g., direct quantification of measurement and discretization errors) and by a separate validation study to characterize the acoustics of the coupler (as opposed to calibrating the coupler).

6 Acknowledgements

The authors thank Li-Chung Chih and Sam Clapp for their contributions to this work.

References

[1] Møller, H., "Fundamentals of binaural technology," *Applied acoustics*, 36(3-4), pp. 171–218, 1992, ISSN 0003-682X, doi:10.1016/0003-682x(92)90046-u.

[2] Zhong, X.-L. and Xie, B.-S., "Head-Related Transfer Functions and Virtual Auditory Display," in H. Glotin, editor, *Soundscape Semiotics - Localisation and Categorisation*, IntechOpen, 2014, ISBN 978-953-51-1226-6, doi:10.5772/56907.

[3] Hammershøi, D. and Møller, H., "Binaural Technique — Basic Methods for Recording, Synthesis, and Reproduction," in *Communication Acoustics*, pp. 223–254, Springer, Berlin, Heidelberg, 2005, ISBN 10.1007/3-540-27437-5_9, doi:10.1007/3-540-27437-5_9.

[4] Prepeliţă, S. T., Bolaños, J. G., Pulkki, V., Savioja, L., and Mehra, R., "Numerical simulations of near-field head-related transfer functions: Magnitude verification and validation with laser spark sources," *The Journal of the Acoustical Society of America*, 148, p. 153, 2020, ISSN 0001-4966, doi:10.1121/10.0001409.

[5] Savioja, L., Prepelită, S., Chobeau, P., and Botts, J., "Can you trust your numeric simulations—How to verify your code and validate your model," *The Journal of the Acoustical Society of America*, 140, p. 3127, 2016, ISSN 0001-4966, doi:10.1121/1.4969790.

[6] Prepeliţă, S. T., Bolaños, J. G., Geronazzo, M., Mehra, R., and Savioja, L., "Pinna-related transfer functions and lossless wave equation using finite-difference methods: Validation with measurements," *The Journal of the Acoustical Society of America*, 147, p. 3631, 2020, ISSN 0001-4966, doi:10.1121/10.0001230.

[7] Roden, R. and Blau, M., "The IHA database of human geometries including torso, head and complete outer ears for acoustic research," in *Internoise 2020*, pp. 1–12, The Korean Society for Noise and Vibration Engineering, Online (Seoul, South Korea), 2020.

[8] Ghorbal, S. and Séguier, X. B. a. R., "Computed Hrirs and Ears Database for Acoustic Research," pp. 13061:1–13061:7, Audio Engineering Society, online, 2020.

[9] Ghorbal, S., Auclair, T., Soladié, C., and Séguier, R., "Pinna morphological parameters influencing HRTF sets," in *Proceedings of the 20th International Conference on Digital Audio Effects (DAFx-17)*, pp. 353–359, Edinburgh, UK, 2017.

[10] Nakazawa, M. and Nishikata, A., "Development of sound localization system with tube earphone using human head model with ear canal," *IEICE Transactions on Fundamentals of Electronics, Communications and Computer Sciences*, E88-A, pp. 3584–3592, 2005, ISSN 17451337, doi:10.1093/IETFEC/E88-A.12.3584.

[11] Walsh, T., Demkowicz, L., and Charles, R., "Boundary element modeling of the external human auditory system," *The Journal of the Acoustical Society of America*, 115, p. 1033, 2004, ISSN 0001-4966, doi:10.1121/1.1643360.

[12] "COMSOL Multiphysics®, v.5.6," 2020.

[13] Cignoni, P., Callieri, M., Corsini, M., Dellepiane, M., Ganovelli, F., and Ranzuglia, G., "MeshLab: an Open-Source Mesh Processing Tool," in V. Scarano, R. D. Chiara, and U. Erra, editors, *Eurographics Italian Chapter Conference*, The Eurographics Association, 2008, ISBN 978-3-905673-68-5, doi:10.2312/LocalChapterEvents/ItalChap/ItalianChapConf2008/129-136.

[14] "ITU-T Recommendation P.57: Artificial ears," pp. 20–35, International Telecommunications Union Standardization Sector, Geneva, Switzerland, 2021.

[15] Harari, I. and Hughes, T. J. R., "Finite element methods for the Helmholtz equation in an exterior domain: Model problems," *Computer Methods in Applied Mechanics and Engineering*, 87, pp. 59–96, 1991, ISSN 0045-7825, doi:10.1016/0045-7825(91)90146-W.

[16] Ihlenburg, F. and Babuška, I., "Finite element solution of the Helmholtz equation with high

wave number Part I: The h-version of the FEM," *Computers Mathematics with Applications*, 30, pp. 9–37, 1995, ISSN 0898-1221, doi:10.1016/0898-1221(95)00144-N.

[17] Oden, J. T., Prudhomme, S., and Demkowicz, L., "A posteriori error estimation for acoustic wave propagation problems," *Archives of Computational Methods in Engineering 2005 12:4*, 12, pp. 343–389, 2005, ISSN 1886-1784, doi:10.1007/BF02736190.

[18] Marburg, S., "Six boundary elements per wavelength: is that enough?" *Journal of Computational Acoustics*, 10(01), pp. 25–51, 2002, ISSN 0218-396X, doi:10.1142/S0218396X02001401.

[19] Schmiechen, P., *Travelling Wave Speed Coincidence*, PhD Thesis, 1997.

[20] Thompson, L. L. and Pinsky, P. M., "Complex wavenumber Fourier analysis of the p-version finite element method," *Computational Mechanics*, 13, pp. 255–275, 1994, ISSN 01787675, doi:10.1007/BF00350228.

[21] Amestoy, P., Duff, I. S., Koster, J., and L'Excellent, J.-Y., "A Fully Asynchronous Multifrontal Solver Using Distributed Dynamic Scheduling," *SIAM Journal on Matrix Analysis and Applications*, 23(1), pp. 15–41, 2001.

[22] Shaw, E. A. G., "Transformation of sound pressure level from the free field to the eardrum in the horizontal plane," *The Journal of the Acoustical Society of America*, 56(6), pp. 1848–1861, 1974, ISSN 0001-4966, doi:10.1121/1.1903522.

[23] Møller, H., Sørensen, M. F., Hammershøi, D., and Jensen, C. B., "Head-Related Transfer Functions of Human Subjects," *Journal of the Audio Engineering Society*, 43(5), pp. 300–321, 1995.

[24] Cheng, C. I. and Wakefield, G. H., "Introduction to Head-Related Transfer Functions (HRTFs): Representations of HRTFs in Time, Frequency, and Space," pp. 5026:1–28, Audio Engineering Society, New York, NY, USA, 1999.

[25] Brinkmann, F., Lindau, A., Weinzierl, S., Par, S. v. d., Müller-Trapet, M., Opdam, R., and Vorländer, M., "A high resolution and full-spherical head-related transfer function database for different head-above-torso orientations," *Journal of the Audio Engineering Society*, 65(10), pp. 841–848, 2017, doi:10/gcr4sr.

[26] Thorpe, J. B. A., *Human Sound Localisation Cues and their Relation to Morphology*, PhD Thesis, The University of York, 2009.

[27] Algazi, V. R., Avendano, C., and Duda, R. O., "Elevation localization and head-related transfer function analysis at low frequencies," *The Journal of the Acoustical Society of America*, 109(3), pp. 1110–1122, 2001, ISSN 0001-4966, doi:10.1121/1.1349185.

[28] Zhong, X.-L. and Xie, B.-s., "Consistency among the head-related transfer functions from different measurements," in *Proceedings of Meetings on Acoustics*, volume 19, pp. 050014:1–050014:5, Acoustical Society of America, 2013, doi:10.1121/1.4799325.

[29] Andreopoulou, A., Begault, D., and Katz, B., "Inter-laboratory round robin HRTF measurement comparison," *IEEE Journal of Selected Topics in Signal Processing*, 9(5), pp. 895 – 906, 2015, ISSN 1932-4553, doi:10.1109/JSTSP.2015.2400417.

[30] Prepeliță, S. T., Gómez Bolaños, J., Geronazzo, M., Mehra, R., and Savioja, L., "Pinna-related transfer functions and lossless wave equation using finite-difference methods: Verification and asymptotic solution," *The Journal of the Acoustical Society of America*, 146(5), pp. 3629–3645, 2019, ISSN 0001-4966, doi:10.1121/1.5131245.

[31] Duda, R. O. and Martens, W. L., "Range dependence of the response of a spherical head model," *The Journal of the Acoustical Society of America*, 104(5), pp. 3048–3058, 1998, ISSN 0001-4966, doi:10.1121/1.423886.

[32] Yu, G.-Z., Xie, B.-S., and Rao, D., "Effect of sound source scattering on measurement of near-field head-related transfer functions," *Chinese Physics Letters*, 25(8), pp. 2926–2929, 2008, ISSN 0256-307X, doi:10.1088/0256-307X/25/8/053.

[33] Spagnol, S., "On distance dependence of pinna spectral patterns in head-related transfer functions," *The Journal of the Acoustical Society of America*, 137(1), pp. EL58–EL64, 2015, ISSN 0001-4966, doi:10.1121/1.4903919.

[34] Huttunen, T., Kärkkäinen, A., Kärkkäinen, L., Kirkeby, O., and Seppälä, E. T., "Some Effects of the Torso on Head-Related Transfer Functions," pp. 7030:1–8, Audio Engineering Society, Vienna, Austria, 2007.

[35] Lentz, T., "Near-field HRTFs," in *Proceedings of Deutsche Jahrestagung für Akustik (DAGA)*, volume 33, pp. 677–678, Stuttgart, Germany, 2007.

[36] Håkansson, B., Carlsson, P., and Tjellström, A., "The mechanical point impedance of the human head, with and without skin penetration," *The Journal of the Acoustical Society of America*, 80(4), pp. 1065–1075, 1986, ISSN 0001-4966, doi:10.1121/1.393848, publisher: Acoustical Society of America.